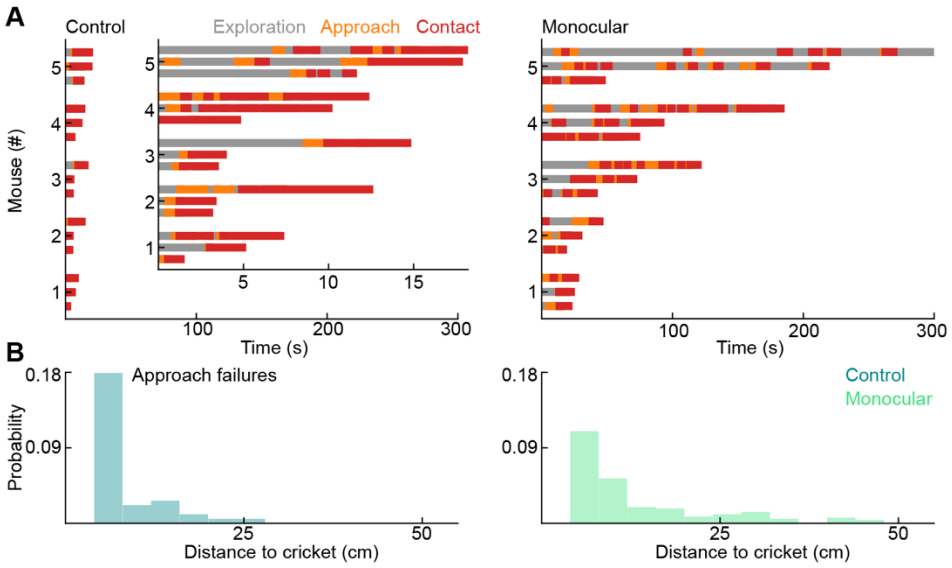


**Figure S1. Monocular mice are poor hunters, Related to Figure 2**

(A) Exploration, approach, and contact over time for all test-day hunting trials of control (left) and monocular mice (right). We recorded three trials for each mouse. Trials are shown grouped by mice ordered by their duration. Mice are ordered by the average duration of their hunting trials.

(B) Distributions of distances at which approaches failed (i.e., ended without contact) in control (left, n = 31 approaches) and monocularly enucleated mice (right, n = 167 approaches, p = 0.0053).

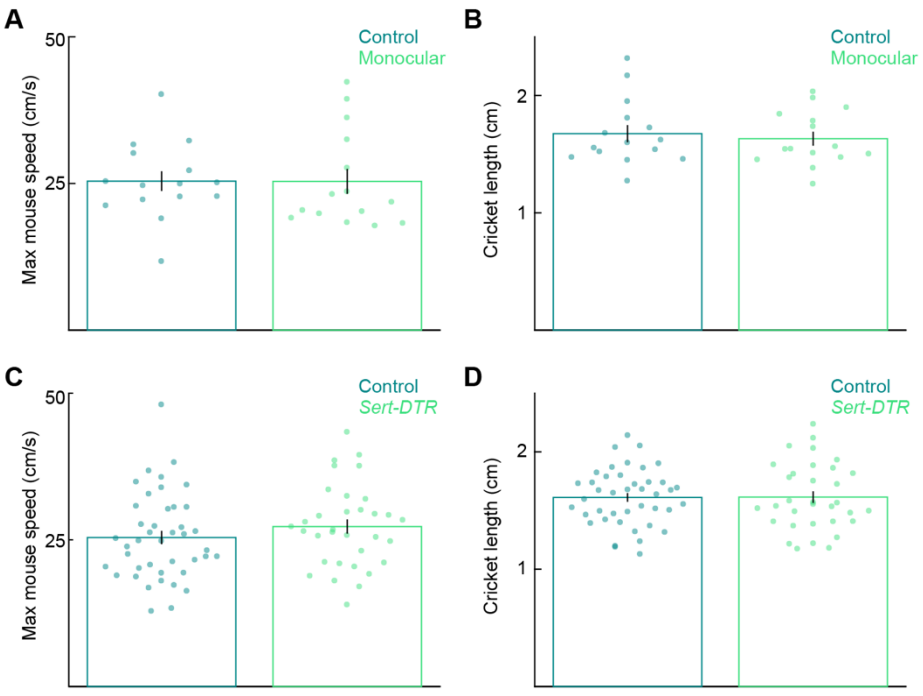


**Figure S2. Mouse running speeds and cricket sizes, Related to Figures 2 and 5**

(A and B) Mouse running speeds and cricket lengths measured from overhead prey capture videos were not significantly different between control and monocularly enucleated mice (A, control: 25.40 ± 6.55 cm/s, monocular: 25.36 ± 8.25 cm/s, p = 0.46; B, control:1.67 ± 0.28 cm; monocular: 1.63 ± 0.23 cm, p = 0.78). (C and D) There were also no significant differences in the size of the crickets hunted between control and *Sert-DTR* mice (D, control:1.61 ± 0.24 cm, *Sert-DTR*: 1.61 ± 0.28 cm, p = 0.95) or the maximum speeds of the mice during hunting (C, control: 25.40 ± 7.35 cm/s, *Sert-DTR*: 27.27 ± 6.99 cm/s, p = 0.22). Error bars represent the standard deviation.

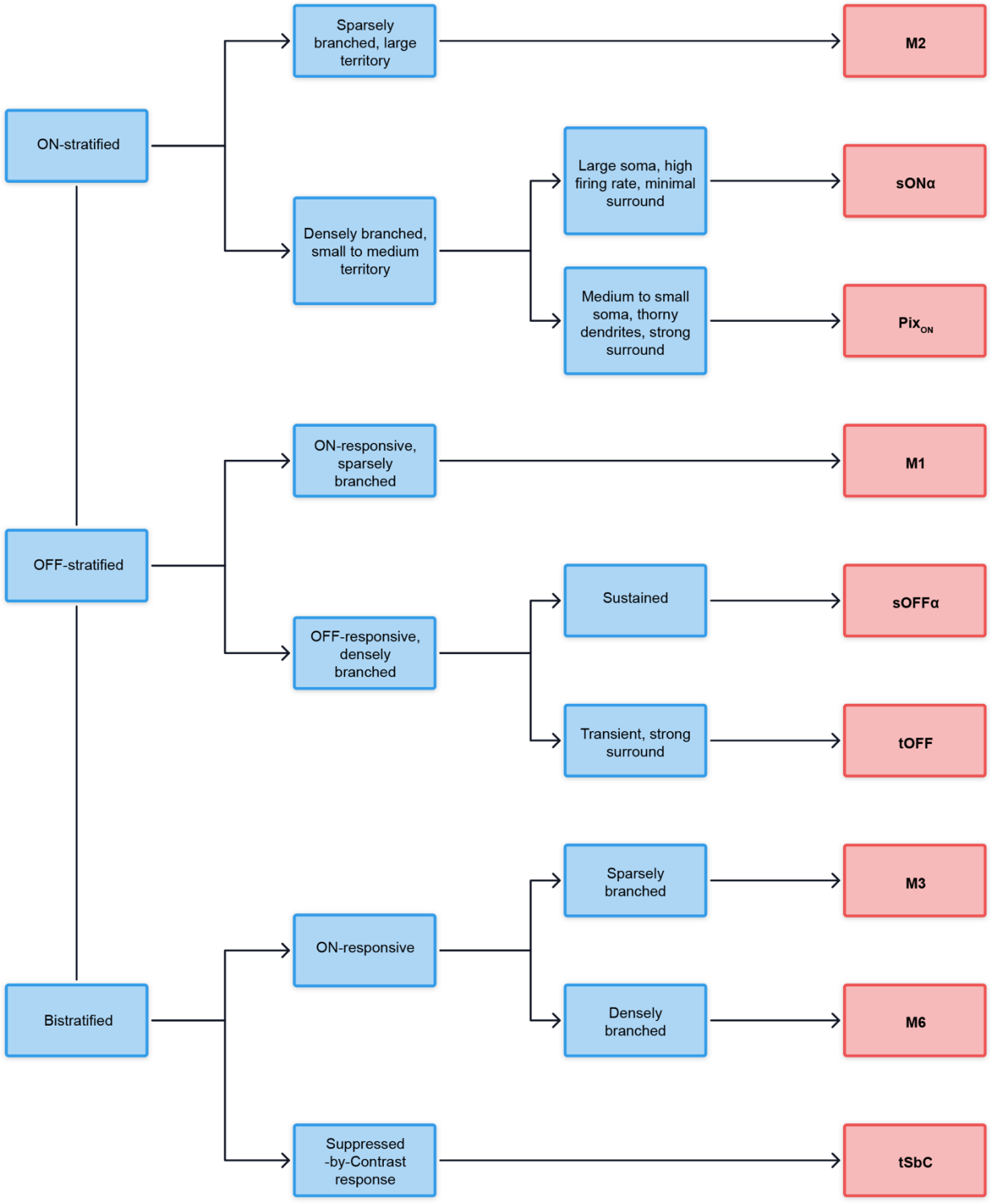


**Figure S3. Classification of ipsi-RGCs based on morphological and functional features, Related to Figure 4**

Flow chart summarizing the classification steps and morphological and functional criteria (baseline firing, varying size spot responses, and drifting grating responses) that divide the ipsi-RGCs into nine types.

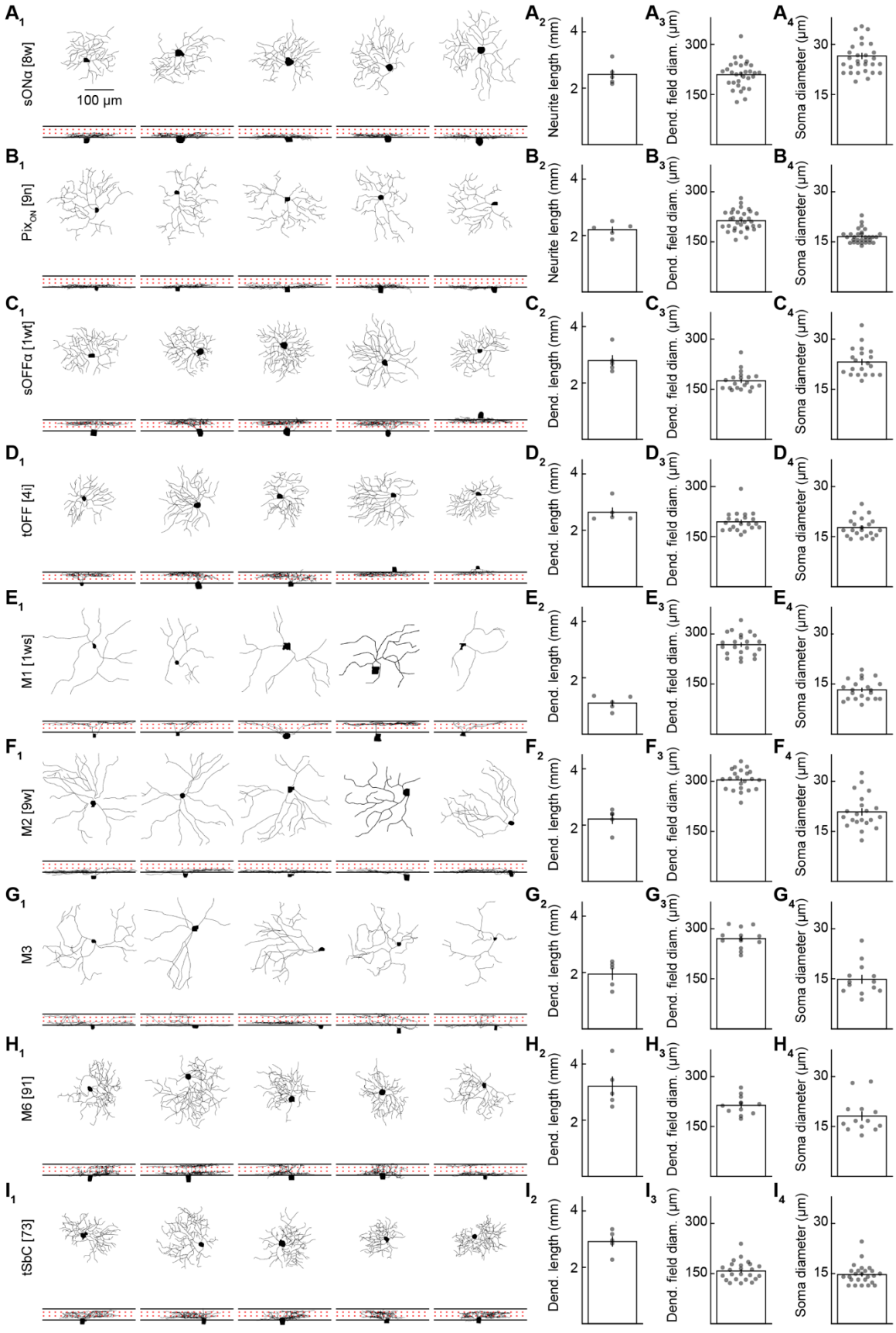
A1
sONα [8w]
100 µm
A2
Neurite length (mm)
A3
Dend. field diam. (µm)
A4
Soma diameter (µm)
B1
PixON [9n]
B2
Neurite length (mm)
B3
Dend. field diam. (µm)
B4
Soma diameter (µm)
C1
sOFFα [1wt]
C2
Dend. length (mm)
C3
Dend. field diam. (µm)
C4
Soma diameter (µm)
D1
tOFF [4i]
D2
Dend. length (mm)
D3
Dend. field diam. (µm)
D4
Soma diameter (µm)
E1
M1 [1ws]
E2
Dend. length (mm)
E3
Dend. field diam. (µm)
E4
Soma diameter (µm)
F1
M2 [9w]
F2
Dend. length (mm)
F3
Dend. field diam. (µm)
F4
Soma diameter (µm)
G1
M3
G2
Dend. length (mm)
G3
Dend. field diam. (µm)
G4
Soma diameter (µm)
H1
M6 [91]
H2
Dend. length (mm)
H3
Dend. field diam. (µm)
H4
Soma diameter (µm)
I1
tSbC [73]
I2
Dend. length (mm)
I3
Dend. field diam. (µm)
I4
Soma diameter (µm)

**Figure S4. Morphology of ipsi-RGC types, Related to Figure 4**

(A-I) Representative traced cells of each ipsi-RGC type ($X_1$, n = 5 traced cells per type). Total dendrite length for the traced cells of each cell type ($X_2$, A: 2.49 ± 0.17 mm, B: 2.21 ± 0.11 mm, C: 2.79 ± 0.20 mm, D: 2.64 ± 0.17 mm, E: 1.10 ± 0.11 mm, F: 2.22 ± 0.17 mm, G: 1.94 ± 0.21 mm, H: 3.20 ± 0.35 mm, I: 2.92 ± 0.18 mm, n = 5 traced cells per type). Dendritic field diameters ($X_3$, A: 209.33 ± 7.26 μm, n = 31, B: 213.19 ± 5.27 μm, n = 30, C: 175.15 ± 6.34 μm, n = 20, D: 194.51 ± 6.43 μm, n = 21, E: 267.99 ± 7.07 μm, n = 21, F: 304.13 ± 6.54 μm, n = 21, G: 270.44 ± 8.15 μm, n = 13, H: 213.41 ± 8.06 μm, n = 13, I: 157.65 ± 5.88 μm, n = 25). Soma diameters ($X_4$, A: 23.53 ± 0.96 μm; B: 15.09 ± 0.38 μm; C: 23.17 ± 0.95 μm; D: 15.70 ± 0.63 μm; E: 13.26 ± 0.65 μm; F: 20.84 ± 1.11 μm; G: 14.85 ± 1.33 μm; H: 18.11 ± 1.41 μm; I: 14.72 ± 0.60 μm, n's same as in $X_3$).

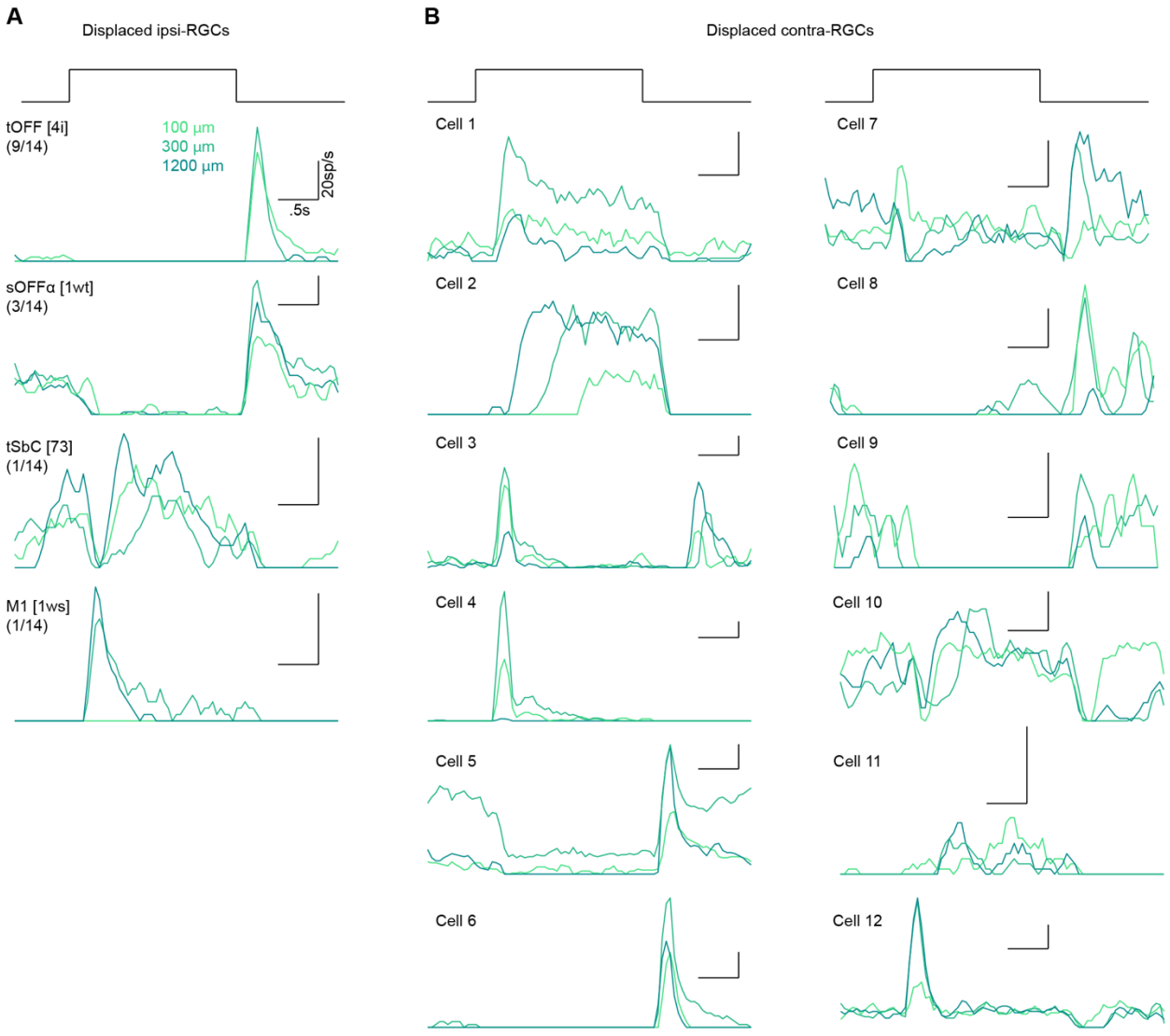


**Figure S5. Light responses of displaced RGCs, Related to Figure 4**

(A) Representative responses of ipsilateral displaced RGCs to spot stimuli (100, 300, 1200 µm). Of the 14 displaced ipsilateral RGCs with sufficient light responses and morphology to classify nine were tOFF-RGCs, three were sOFFα-RGCs, one was an M1-RGC, and one was a tSbC-RGC. In addition, one ON-stratifying RGC with poor light responses and morphological reconstruction was recorded. (right).

(B) Responses of all 12 recorded displaced contralateral RGCs. Contralateral displaced RGCs showed diverse response types (ON-sustained, ON-transient, ON-delayed, OFF-sustained, OFF-transient, ON-OFF, and SbC), including many found in neither the displaced ipsi-RGCs nor the ipsi-RGCs in the GCL. All recorded INL cells spiked and had axons that ran through the INL to the GCL and towards the optic nerve, suggesting all recorded cells were displaced RGCs.

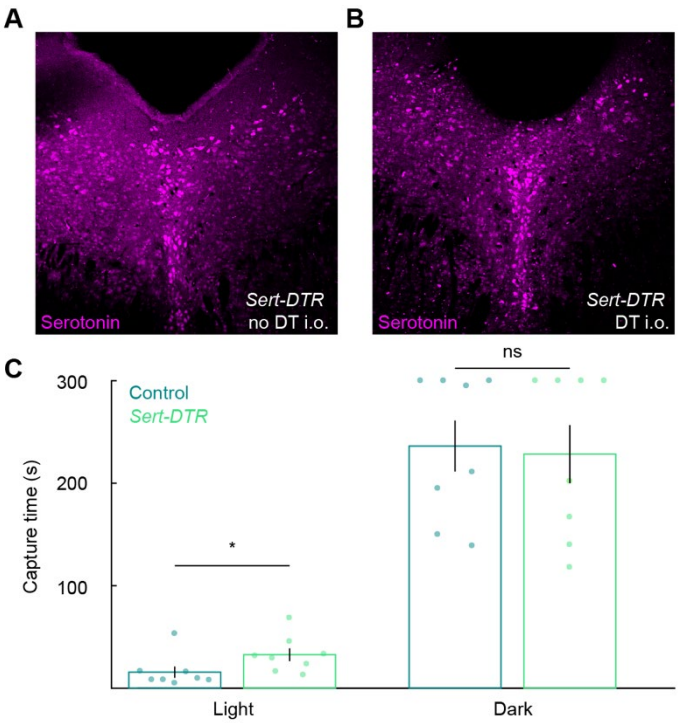


**Figure S6. Intraocular DT injections do not ablate serotonergic neurons in the brains of *Sert-DTR* mice, Related to Figure 5**

(A and B) Representative images of coronal vibratome slices through the dorsal raphe nucleus of the brains of *Sert-DTR* mice injected intraocularly with DT (B) or not (A).

(C) We tested the ability of a subset of DT-injected control and *Sert-DTR* mice to hunt crickets in the dark. Following prey capture tests in the light on the fifth day (see STAR Methods), food deprivation was extended and hunting success in the dark tested on the sixth day. Whereas the removal of ispi-RGCs significantly increased capture times in the light (control: 15.66 ± 5.56 s, n = 8, *Sert-DTR*: 32.69 ± 6.29 s, n = 8, p = 0.020), it had no effects on the cricket capture times of the same mice in the dark (control: 236.25 ± 24.96 s, n = 8, *Sert-DTR*: 228.38 ± 28.34 s, n = 8, p = 1). This indicates that the poor prey capture performance of DT-injected *Sert-DTR* mice is due to their visual deficits. The long cricket capture times of both groups of mice in the dark suggest that, in our experimental conditions (including padded flooring in the arena and limited noise isolation of the behavior room) (Hoy et al., 2016), other senses are unable to guide efficient prey capture.

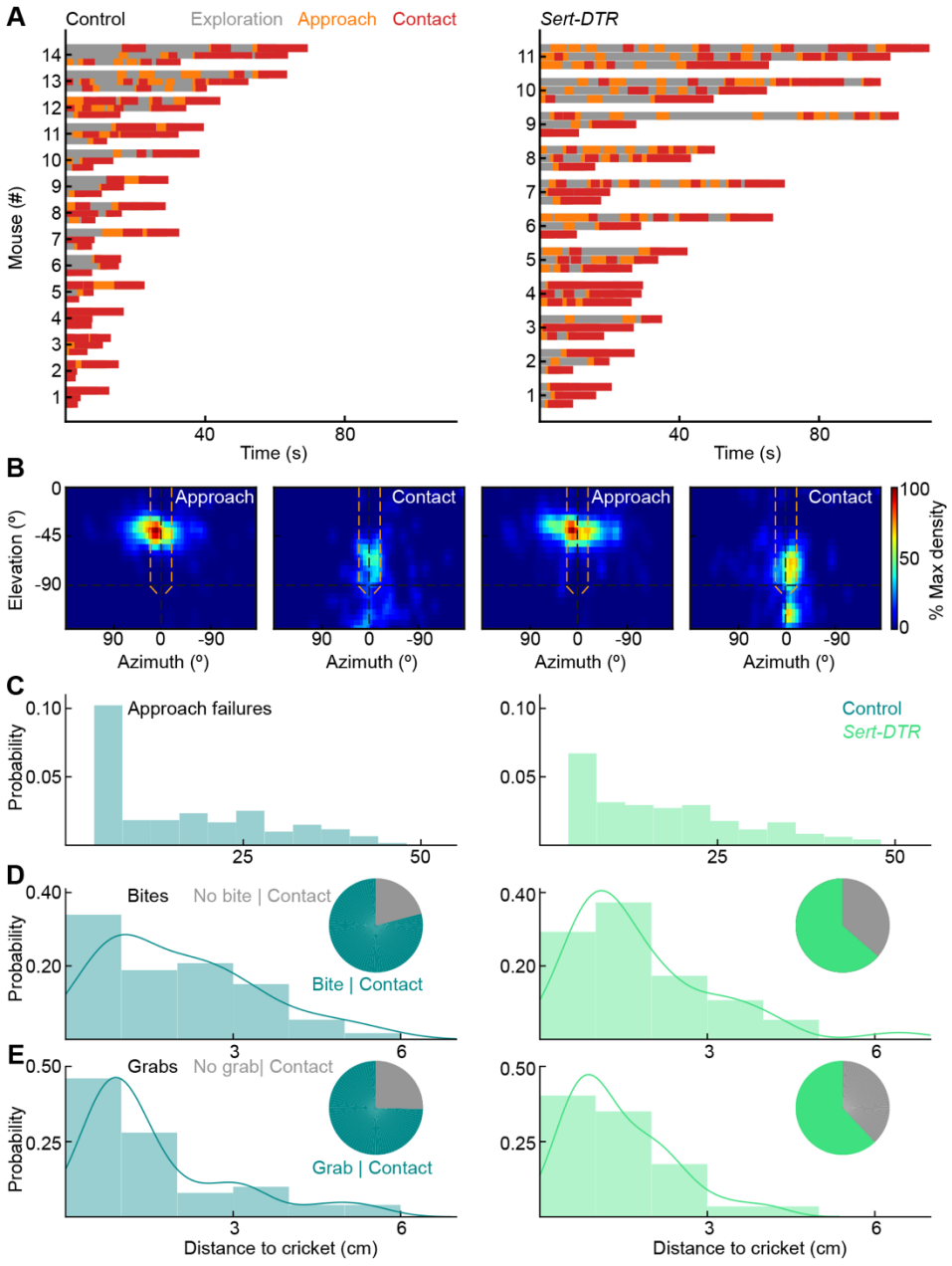


**Figure S7. Ipsilaterally projecting RGCs are required for efficient prey capture, Related to Figure 5**
(A) Exploration, approach, and contact over time for all test-day hunting trials for DT-injected control (left) and *Sert-DTR* mice (right). We recorded three trials for each mouse. Trials are shown grouped by mice ordered by their duration. Mice are ordered by the average duration of their hunting trials.
(B) Heatmaps of the cricket positions during the approach and contact phases of hunting of DT-injected control (left, n = 4 hunts) and *Sert-DTR* mice (right, n = 4 hunts).
(C) Distribution of distances at which approaches failed (i.e., ended without contact) in DT-injected control (left, n = 107 approaches) and *Sert-DTR* mice (right, n = 205 approaches, p = 0.0065).

(D) Distance distributions of bites in DT-injected control (left, n = 53 bites in 67 contacts) and *Sert-DTR* mice (right, n = 77 bites in 121 contacts, p = 0.25). Inset pie charts show the frequency of bites per contact in DT-injected control (left) and *Sert-DTR* mice (right, p = 0.028).
(E) Distance distributions of grabs in DT-injected control (left, n = 50 grabs in 67 contacts) and *Sert-DTR* mice (right, 75 grabs in 121 contacts, p = 0.67). Inset pie charts show the frequency of grabs per contact in DT-injected control (left) and *Sert-DTR* mice (right, p = 0.078).

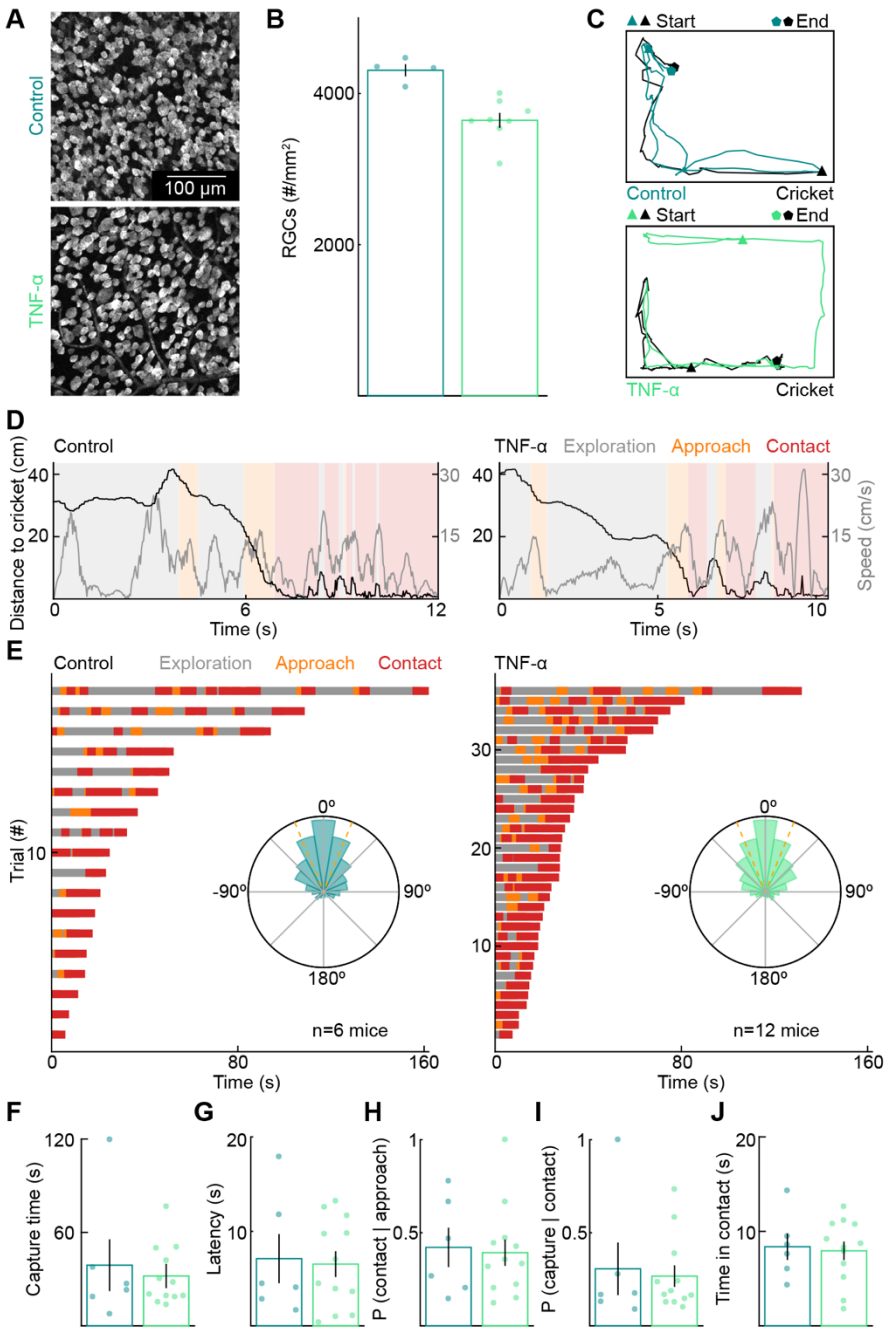


**Figure S8. Removal of ~15% of RGCs by TNF-α does not affect prey capture performance, Related to Figure 5**

(A) Representative images of control (saline-injected) (top) and TNF-α injected (bottom) retinas with RGCs labeled by RBPMS staining.

(B) Four images (one from each quadrant) per retina were counted using Cellpose (Stringer et al., 2020). Each dot shows the average density across the four quadrants of one retina, which was reduced by ~15% in TNF-α injected retinas (control: 4307.10 ± 80.45 RGCs/mm$^2$, TNF-α: 3644.71 ± 98.92 RGCs/mm$^2$, p = 0.004).

(C) Representative tracks of mouse and cricket positions in control (top) and TNF-α-injected mice (bottom).

(D) Same hunts as in (A) showing the distance to cricket and mouse speed in the three hunting phases.
(E) Exploration, approach, and contact over time for all test-day hunting trials for control (left) and TNF-α (right). Insets: circular histograms of the cricket azimuth during approaches across all control (left) and enucleated (right) mice ($p = 1$).
(F) Time from the introduction of cricket to its capture (control: 38.94 ± 16.64 s, TNF-α: 32.03 ± 5.53 s, $p = 0.91$). Mice in both groups were slower than controls in monocular enucleation (Figure 2) and *Sert-DTR* (Figure 5) experiments. This may be due to the older age of mice in the experiments presented in this figure due to the time required (approximately six weeks) for TNF-α actions to unfold.
(G) Latency to detect prey and initiate first approach (control: 7.11 ± 2.60 s, TNF-α: 6.54 ± 1.37 s, $p = 0.89$).
(H) Probability that mice successfully convert approaches into contacts (control: 0.43 ± 0.11, TNF-α: 0.40 ± 0.07, $p = 0.84$).
(I) Probability that mice successfully convert contacts into captures (control: 0.31 ± 0.14 s, TNF-α: 0.27 ± 0.06 s; $p = 0.96$).
(J) Total time within contact range of the cricket before successful capture (control: 9.25 ± 1.75 s, TNF-α: 7.99 ± 0.99 s, $p = 0.75$).